Since January 2020 Elsevier has created a COVID-19 resource centre with free information in English and Mandarin on the novel coronavirus COVID-19. The COVID-19 resource centre is hosted on Elsevier Connect, the company's public news and information website.

Biosensors and Bioelectronics 172 (2021) 112747

Contents lists available at ScienceDirect

Biosensors and Bioelectronics

journal homepage: http://www.elsevier.com/locate/bios

Long period grating in double cladding fiber coated with graphene oxide as high-performance optical platform for biosensing

Flavio Esposito [a,1], Lucia Sansone [b,1], Anubhav Srivastava [a], Francesco Baldini [c], Stefania Campopiano [a], Francesco Chiavaioli [c,*], Michele Giordano [b,**], Ambra Giannetti [c,2], Agostino Iadicicco [a,2]

[a] Department of Engineering, University of Naples "Parthenope", Centro Direzionale Isola C4, 80143, Napoli, Italy
[b] Institute for Polymers, Composites and Biomaterials, National Research Council of Italy (CNR), 80055, Portici, Italy
[c] Institute of Applied Physics "Nello Carrara", National Research Council of Italy (CNR), 50019, Sesto Fiorentino, Italy

ARTICLE INFO

Keywords:
Label-free biosensors
Real-time biomolecule detection
Double cladding fiber sensors
Graphene oxide
Long period gratings
C-Reactive protein

ABSTRACT

In this work, the development and testing of a novel fiber-optic based label-free biosensor is presented, whose performance were verified through the detection of C-reactive protein (CRP) in serum. The device is based on a long period grating fabricated in a double cladding fiber with a W-shaped refractive index (RI) profile. As a result, the working point of the device was tuned to the mode transition region by chemical etching of the outer fiber cladding, obtaining a significant enhancement of the RI sensitivity and an excellent visibility of the grating resonances due to the mode transition in an all-silica structure. The fiber transducer was coated with a nanometric thin layer of graphene oxide in order to provide functional groups for the covalent immobilization of the biological recognition element. A very low limit of detection of about 0.15 ng/mL was obtained during the detection of CRP in serum, and a large working range (1 ng/mL – 100 μg/mL) of clinical relevance has been also achieved.

1. Introduction

In the great many of biosensors based on fiber-optics, the engineering of the devices able to maximize the refractive index (RI) sensitivity, and hence to enhance the limit of detection (LOD), is often achieved impairing signal stability, repeatability and signal-to-noise ratio (SNR). One of the most appropriate example is given by long period grating (LPG) based devices which played a leading role in the scenario of fiber-optic biosensors (Chiavaioli et al., 2017a; Esposito et al., 2020a). An LPG consists of a few centimeter long optical fiber with periodic perturbation in its refractive index and/or geometry, where period typically ranges from 100 to 1000 μm (James and Tatam, 2003). The grating induces the coupling between the light from the fundamental core mode (of a single mode fiber) to forward propagating cladding modes. As a result, discrete attenuation bands are visible in the fiber transmission spectrum, located at those wavelengths $\lambda_{res,i}$ satisfying the phase-matching condition given by (James and Tatam, 2003; Shu et al., 2002):

$$\lambda_{res,i} = \left(n_{eff,co} - n_{eff,cl}^{(i)}\right)\cdot\Lambda \quad (1)$$

where $n_{eff,co}$ and $n_{eff,cl}^{(i)}$ are the effective refractive index of the core mode and the i-th cladding mode, respectively, while Λ is the grating period. The LPG finds large interest in bio-chemical sensing due to the intrinsic sensitivity to the surrounding refractive index (SRI) of the cladding modes. The sensing principle behind this kind of technology platforms lies in the measurement of changes in the surface refractive index stemming from the binding interaction between a biological recognition element (BRE) grafted onto the fiber surface and the analyte under investigation (Chiavaioli et al., 2017b). However, suitable strategies are necessary in order to increase the sensitivity and selectivity (Chiavaioli et al., 2014a, 2015; Del Villar, 2015; Shu et al., 2002; Śmietana et al., 2016). The mode transition phenomenon promotes high SRI sensitivity,

* Corresponding author.
** Corresponding author.
E-mail addresses: f.chiavaioli@ifac.cnr.it (F. Chiavaioli), michele.giordano@cnr.it (M. Giordano).
[1] These authors have to be both considered as first author.
[2] These authors have to be both considered as last author.

https://doi.org/10.1016/j.bios.2020.112747
Received 21 May 2020; Received in revised form 11 October 2020; Accepted 18 October 2020
Available online 22 October 2020

in turn achieving very low limits of detection. However, it demands the deposition of a high RI (HRI) overlay onto LPG region, which can affect the visibility of the attenuation bands, long term stability and repeatability of the device. In particular, the resonance depth can be reduced even to few dB during mode transition (Biswas et al., 2016; Del Villar et al., 2005).

To address the following challenges, a device based on an unconventional long period grating fabricated in a double cladding fiber (DCF) with a W-shaped refractive index profile has been proposed here. As exemplary analyte to verify its performance, attention was focused on C-reactive protein (CRP), a relevant biomarker involved in several pathologies, which has been widely investigated. It is a homopentameric protein composed by five-polypeptide subunits (23 kDa each) non-covalently associated in a ring configuration. The level of CRP in serum in healthy Caucasian people is estimated to be around 0.8 μg/mL (Sproston and Ashworth, 2018); nevertheless, many factors can alter this value, such as age, gender, smoking status, weight, lipid levels, and blood pressure (Hage and Szalai, 2007). CRP is then considered a serum biomarker for infection or inflammation during which its concentration can rise up to 1000-fold as a consequence of some bacterial infections (Aray et al., 2016; Sproston and Ashworth, 2018). Moreover, constantly high concentration of CRP, rather than spikes of it, has been associated to cardiovascular diseases (CVDs) and to atherosclerosis (Nathan and Ding, 2010). The clinical significance of CRP has been also evaluated for type 2 diabetes mellitus, age-related macular degeneration, hemorrhagic stroke, Alzheimer's disease, and Parkinson's disease (Luan and Yao, 2018). Finally, very recently, it has been demonstrated that CRP levels could reflect COVID-19 disease severity and could be used as a key indicator for the monitoring of such disease (Wang, 2020). In this frame of diseases, in which increasing concentration of CRP is involved, the importance of having a reliable, affordable, and sensitive device for CRP quantification became evident.

The commercially-available optical system for CRP measurements, at the moment, is the well consolidated enzyme-linked immunosorbent assay (ELISA) method, with which a LOD of about 10 pg/mL has been reached (Thermofisher Scientific, n. d.). Other methods are based on different techniques such as immunoturbidimetric or immunonephelometry assay reaching 0.03 μg/mL and 0.2 μg/mL, respectively (Clarke et al., 2005; Dominici et al., 2004; Parra et al., 2005). Different fiber-optic biosensors have been also reported until now for the detection of CRP (Salvo et al., 2017). Among them, those based on surface plasmon resonance (SPR) are widely employed: for example, in 2016 a low limit of detection of 0.009 μg/mL was obtained in serum with a plastic optical fiber-based device (Aray et al., 2016), whereas one year later a single-ended device was reported, which was tested for CRP concentrations down to 0.01 μg/mL in serum (Wang et al., 2017). Fiber grating sensors have been also employed for this purpose. In 2015, an etched fiber Bragg grating (eFBG) coated with anti-CRP antibody - graphene oxide (GO) complex, was reported with a LOD of 0.01 μg/mL in serum (Sridevi et al., 2015). More recently, with the same eFBG technology, a very low LOD of 0.82 fg/mL was obtained in modified buffer solution (Schulze et al., 2018). Furthermore, the physical phenomenon of lossy mode resonance (LMR) has been applied for the detection of CRP, where an Indium Tin Oxide (ITO)-coated D-shaped fiber device attained a LOD of 0.0625 μg/mL in tri-buffer solution (Zubiate et al., 2017). Finally, other technologies have also been exploited achieving remarkable LODs, such as, for example, chemiluminescence-based sensor (Islam and Kang, 2011), where a LOD of 0.2 pg/mL in serum was attained.

The latest trends in nanomaterials for biosensing see the investigation of the properties of graphene oxide (Hernaez et al., 2017). The hydrophilic nature of GO, deriving from the oxygen-containing functional groups, gives good water dispersibility and biocompatibility, which are highly important features in bio-applications. Due to its favorable intrinsic properties, it has been employed for the development of various types of biosensors based on electrochemistry, optics (fluorescence, colorimetry, and Raman), and mass analysis (Liu et al., 2012; Wang et al., 2011). Currently, only few papers have reported about the integration of GO with LPG technology (Esposito et al., 2018b; Liu et al., 2018; Xu et al., 2020).

Very recently, an unconventional device working in mode transition region and capable of providing both high sensitivity and excellent SNR has been proposed (Esposito et al., 2020b; Giordano et al., 2020). On these bases, in this work an LPG in a DCF with W-shaped RI profile empowered to induce the mode transition phenomenon in all-silica fiber, thus improving the grating spectral features, has been designed, developed and characterized. The grating was coated with a nanometric thin layer of GO exhibiting functional groups (such as carboxylic groups) for the covalent immobilization of the capture antibody. Finally, the developed system was tested towards the detection of CRP in serum using CRP concentrations of clinical relevance.

2. Materials and methods

2.1. Chemicals

Hydrofluoric acid (HF), Sodium nitrate ($NaNO_3$), Potassium permanganate ($KMnO_4$), Sulfuric acid (H_2SO_4), Hydrogen peroxide (H_2O_2) were supplied by Sigma Aldrich (Italy). 1-ethyl-3-(3-dimethylaminopropyl)carbodiimide (EDC) and N-hydroxysuccinimide (NHS) were purchased from Life Technologies Italia (Monza, Italy). C-reactive protein (CRP), purified antigen, was purchased from Biodesign (Saco, USA). The mouse monoclonal antibody anti-CRP, clone C5, was from Meridian Life Science (Memphis, USA). Human serum (C Reactive Protein Free Serum) was purchased by HyTest Ltd. (Turku, Finland). All the other reagents, including those for phosphate buffered saline (PBS, 40 mM, pH 7.4) and bovine serum albumin (BSA), were purchased from Merck Life Science (Milano, Italy).

2.2. Graphene oxide preparation and characterization

Graphene oxide is a chemically modified graphene that is typically prepared by oxidation and exfoliation of graphite-bearing oxygen functional groups, such as carboxyl (-COOH), hydroxyl (-OH), or epoxy (-O-), on their basal planes and edges with the modified Hummers' method (Hummers and Offeman, 1958; Rourke et al., 2011).

Here, a small amount of flake graphite (average particle diameter of 5 nm, 99.75% purity, Asbury Carbons, U.S.A.) was vigorously stirred for 5 days in a solution of $NaNO_3$ and $KMnO_4$ in concentrated H_2SO_4, washed with H_2SO_4 (5% wt) and subsequently with a solution of H_2O_2 (30% wt) to complete the oxidation. Inorganic anions and other impurities were removed through washing cycles that included centrifugation, discarding supernatant liquid and suspending the solid in an aqueous mixture of 3% wt H_2SO_4 and 0.5% wt H_2O_2 using stirring and ultrasonication. For GO layer fabrication, 10 mg of powder was first suspended in 5 mL of water by ultrasonication and then centrifuged at 14,000 rpm to remove multilayer species. Finally, the GO solution was diluted at a concentration of 2 mg/mL.

XE-100 Atomic Force Microscopy (AFM, Park Systems) was used for the imaging of GO sheets deposited on glass substrate. Surface imaging was obtained in noncontact mode using silicon/aluminum coated cantilevers (PPP-NCHR 10M; Park Systems) 125 μm long with resonance frequency of 200–400 kHz and nominal force constant of 42 N/m. The scan frequency was typically 1 Hz per line. Fig. 1(a) shows the AFM image of GO deposited on glass slide and the corresponding profile measurement. Nanosheets with different sizes ranging from few tens of nanometers to hundreds of nanometers can be observed. Profile measurement demonstrated the presence of sheets up to 4 nm thick.

The nanostructure morphology analysis of GO deposited on an optical fiber tip (as similar substrate but easier in handling during the imaging) was conducted by means of scanning electron microscopy (SEM FEI Quanta 200 FEG). From the SEM images showed in Fig. 1(b), it

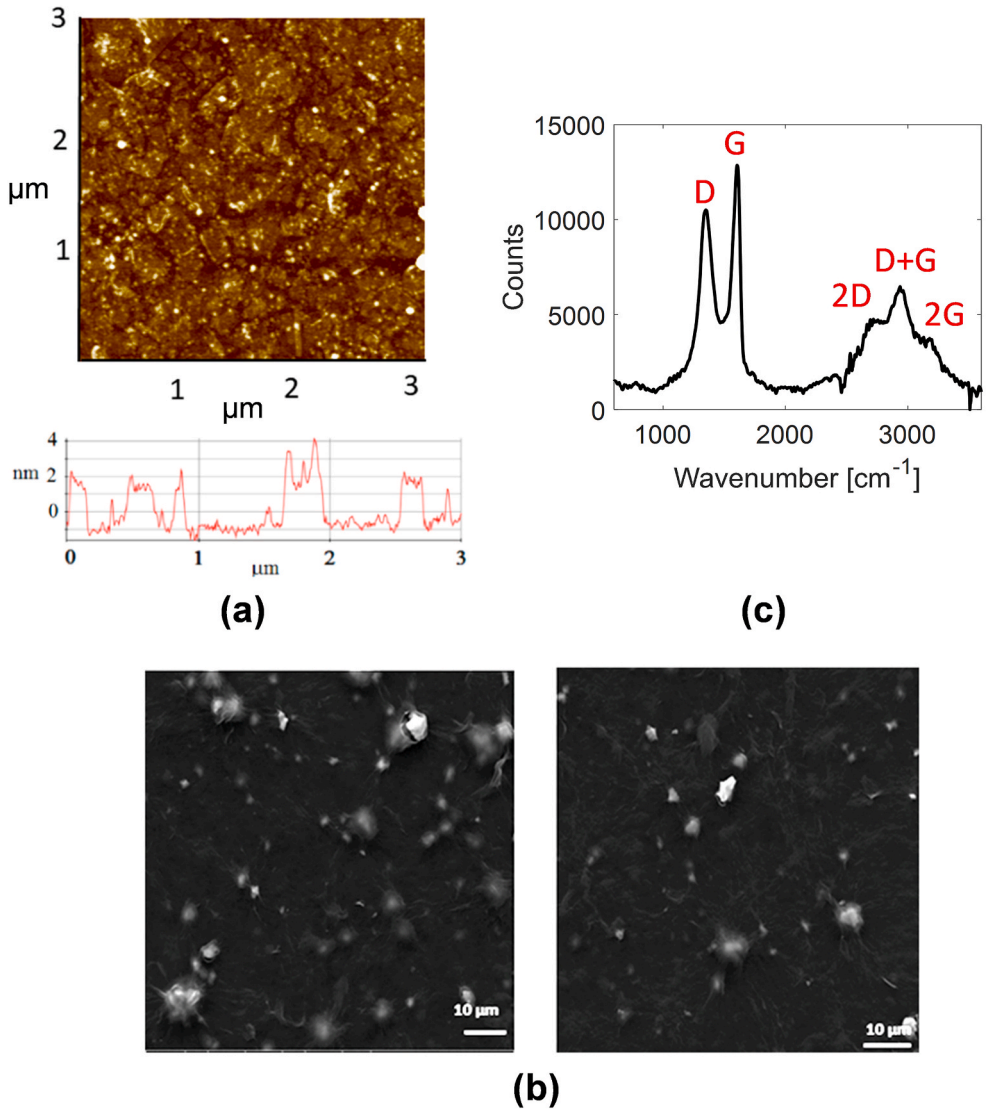

Fig. 1. (a) AFM image of graphene oxide deposited on glass slide and corresponding profile measurement. (b) SEM images of GO deposited onto the optical fiber tip. (c) Raman spectrum of GO coated on a glass slide. (For interpretation of the references to color in this figure legend, the reader is referred to the Web version of this article.)

is evident that GO has a multiple lamellar layer structure and it is possible to distinguish the edges of individual sheets. The films are stacked one above the other and show wrinkled areas. The individual GO sheets were found to have a width of 1–2 µm. Moreover, from the EDX analysis, the graphene oxide contains around 66.52 @% C, 32.72 @ % O and 0.76 @% S.

The nanostructure of GO was also confirmed by Raman Spectroscopy, through a Renishaw inVia Reflex Raman spectrometer (UK) using a 514.5 nm excitation source. The Raman spectrum of GO film on a glass slide substrate is detailed in Fig. 1(c), and it displays a D band at ~1340 cm^{-1} and a broad G band at ~1580 cm^{-1}. The D peak generates from the structural imperfections created by the attachment of hydroxyl and epoxide groups on the carbon basal plane. The G peak duly corresponds to the first order scattering of the E_2G phonon mode of sp^2 C atoms. The intensity of 2D-band at ~2700 cm^{-1} with respect to the D and G peaks is small, due to disorder and multilayer materials (Zhu et al., 2010).

For the purpose of the work, the 2 mg/mL GO water dispersion, prepared according to the mentioned procedure, was deposited on the transducer surface by dip coating technique using a withdrawal speed of 100 mm/min (Esposito et al., 2018b).

2.3. Optical transducer

The optical transducer proposed in this work consists of an unconventional LPG written in DCF (model S1310, manufactured by Nufern, USA) with W-type RI profile exploiting the mode transition phenomenon (Esposito et al., 2020b), coated with nanometric layer of graphene oxide, as schematically reported in Fig. 2.

The W-type fiber presents an outer cladding with refractive index higher than inner one: some cladding modes can be guided in the outer ring-shaped cladding without interacting with the core mode. However, through the chemical etching of the fiber (i.e. decreasing of the external cladding thickness) the transition phenomenon from outer-to inner-cladding of those modes can be induced. As a matter of fact, the mode transition phenomenon is achieved in all-silica fiber, achieving a significant enhancement of the SRI sensitivity while preserving the band visibility, with consequent improvement in the resonance wavelength detection and SNR.

The device is subsequently coated with a thin layer of GO in order to provide functional groups on the sensor surface for the BRE grafting process.

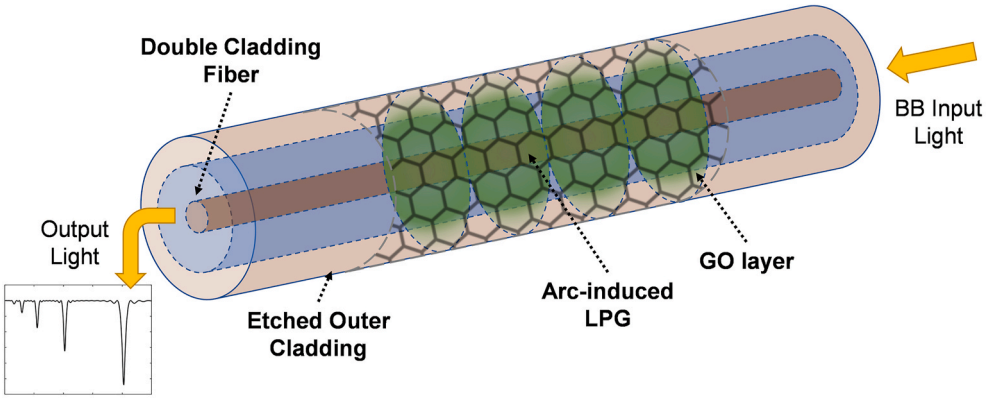

Fig. 2. Schematic view of the optical transducer based on LPG in DCF coated with GO. (For interpretation of the references to color in this figure legend, the reader is referred to the Web version of this article.)

2.4. Experimental setup

Fig. 3 shows a graphical representation of the entire experimental setup used for the detection of the CRP. The fiber-optic sensor is embedded into a thermally-stabilized microfluidic system thanks to the use of Peltier cells (3 in series; each cell: 15 × 30 mm, 7.6 V, 3.9 A, 17.9 W). The microfluidic system that is similar to that used in previous publications (Chiavaioli et al., 2014a, 2015, 2018) is made of two bars: the bottom one is in stainless steel and in contact with the Peltier cells due to the inherent thermal features of the material; the top one is in poly(methyl methacrylate) (PMMA) in order to guarantee the visual inspection of the fluidic channel during the measurement. Both bars possess a lateral hole in the center with a diameter of 2 mm that allows housing a thermocouple: in the case of the bottom bar, it represents the temperature control necessary to provide the feedback for the electronic driver (ILX Lightwave LDC-3722B TEC controller) that controls the Peltier cells; in the case of the top bar, it serves to provide the temperature value inside the fluidic channel through a thermometric unit (Lutron TM-917). The fluidic channel, with dimensions of 1 mm^2 in section and 40 mm in length, contains a volume of roughly 40 μL and is engraved in the center of the two bars, whilst the top bar also incorporates two V-shaped grooves on both edges with a depth of roughly 0.3 mm. These grooves allow fixing the fiber through an optical glue (NOA 68, Norland) that polymerizes with ultraviolet light in 15/20 min. The two bars are held together by a system of 8 screws, whilst a wax film (PARAFILM "M") with a width of 5 mm and a length of 10 mm is interposed between the two bars with a central opening (1 mm × 4 mm) that mimics the fluidic channel. This wax film allows to avoid any kind

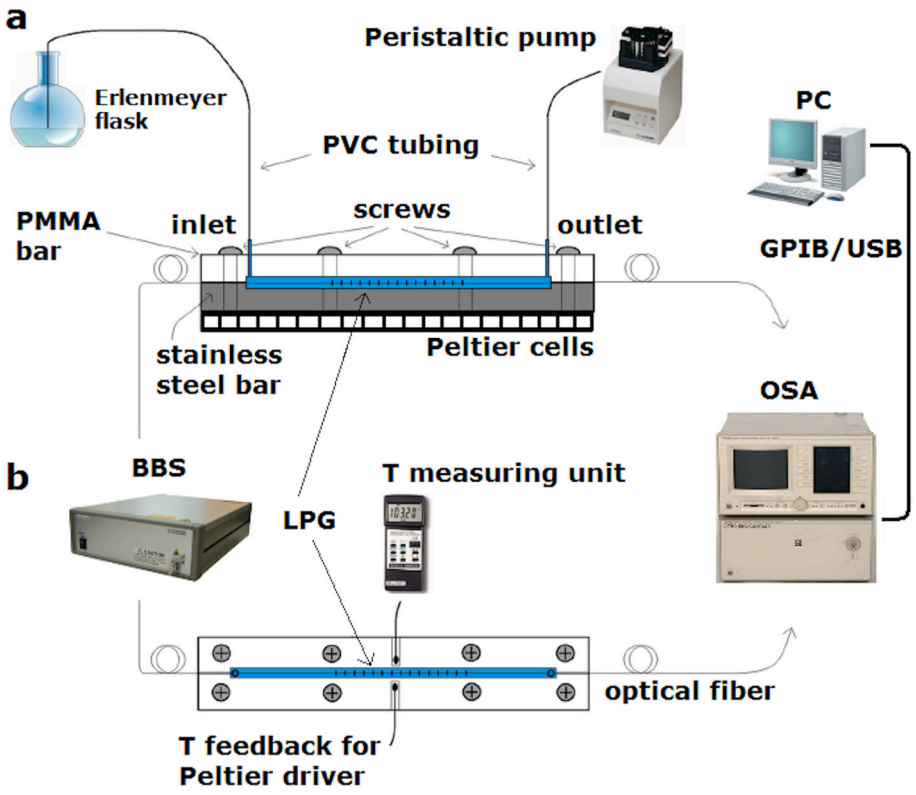

Fig. 3. Sketch of the entire experimental setup together with the microfluidic system in both its (a) cross-section and (b) top views. BBS: broadband optical source; LPG: long period grating; OSA: optical spectrum analyzer. (For interpretation of the references to color in this figure legend, the reader is referred to the Web version of this article.)

of leakage inside the fluidic channel and to inject the solution by a peristaltic pump (GILSON Minipuls 3) from an inlet to an outlet (stainless steel tubes with external diameter of 1.2 mm) with a fixed flow rate, thus avoiding the formation of air bubbles.

As far as the optical part concerns, a broadband optical source (BBS; FIBRELABS, Inc., SLD1310/1430/1550/1690) is used to launch the light into the fiber and an optical spectrum analyzer (OSA; Anritsu MS9030A/MS9701B) collects the light in order to monitor in real time the variations of the optical signal in the band of interest. All the optical fibers were properly fixed during the experiments to avoid any polarization-induced effect. OSA is then connected via GPIB IEEE 488/USB interface to a laptop that allows to record the optical spectrum of the signal and the variation of the $\lambda_{res,i}$ with a resolution of 0.01 nm and an accuracy of 0.007 nm (Chiavaioli et al, 2015, 2017b) through a software created ad hoc using LabWindowsTM/CVI (National Instruments).

2.5. Receptor immobilization and assay protocol for CRP detection

The GO thin layer, which has been deposited onto the fiber surface, directly provides the –COOH functional groups, which are used for the covalent immobilization of the capture antibody, without the need for any additional functional layer (i.e. silane, polymer, etc.). In fact, with outstanding chemical stability and large surface area, GO consists of carbon atoms featured in two dimensional honeycomb lattice structure, containing both sp^2- and sp^3-hybridized carbon atoms as well as functional groups such as hydroxyl, epoxy, carboxyl on its basal plane and sheet edges, which can be used for immobilization of biomolecules. The enriched functional groups can interact in an ionic, electrostatic or, the strongest way, in a covalent manner, so that in principle they provide the highest extraction efficiency of biomolecules per unit area (Loh et al., 2010). The –COOH groups of GO were activated by cross-linking chemistry with 200 mM EDC and 50 mM NHS for 30 min. The covalent immobilization of the receptor for CRP (monoclonal antibody clone C5, 500 μg/mL) was allowed to react for 1 h at a very slow flow rate of 15 μL/min. The unreacted antibodies were removed washing for 10 min with PBS at a faster flow rate of 150 μL/min. The surface passivation was obtained with 1% (w/v) of BSA in PBS, treating the surface for 20 min and then washing for 10 min in PBS. The passivation step is useful in order to block the remaining activated carboxylic groups, so as to prevent non-specific adsorption onto the surface (Berneschi et al., 2017; Giannetti et al., 2020; Lichtenberg et al., 2019; Pisco and Cusano, 2020; Vaiano et al., 2016; Zubiate et al., 2019).

The CRP calibration curves were obtained performing analyte binding steps, with increasing concentrations of CRP within the range 0.01–100 μg/mL in real samples of human serum (diluted 1:10 (v/v) in PBS) for 20/30 min at a slow flow rate of 25 μL/min, followed by a washing step with PBS for 10/15 min. In both cases, the duration of each step has been adjusted depending on the time necessary to reach the steady state in chemical kinetics during the binding interaction. During the entire assay protocol, the temperature of the control system described in the previous section was set at (26 ± 0.05) °C.

3. Results and discussion

The evaluation of the wavelength shift of the resonance ($\lambda_{res,i}$) in the transmission spectrum, which is generated through the inscription of a long period grating in double cladding fiber and the exploitation of the mode transition phenomenon in guided-optics, permits to accurately detect antibody/antigen interactions. In addition, the deposition of a nanometric film of graphene oxide allows a direct functionalization of the fiber surface due to the presence of carboxylic groups. The operation principle lies in monitoring in real time the interaction between the receptor (anti-CRP, clone C5) – the so-called capture antibody – grafted on the functionalized surface of the fiber, and the specific target analyte (CRP), which produces changes in both the thickness and the RI of the sensing bio-layer. When the target analyte binds the receptor, a shift towards shorter wavelengths – hereafter called blue-shift – occurs in accordance with Equation (1) (Chiavaioli et al., 2017a, 2017b). In the next sections, the details of the fabrication of the optical transducer (section 3.1), of the preparation of the sensing bio-layer (section 3.2) and of the detection of CRP in real samples (section 3.3) are provided. The repeatability and reproducibility of the entire process (encompassing device fabrication, assay protocol and device response) are underpinned by independent tests carried out in the same experimental conditions and with use of similar devices.

3.1. Fabrication of the optical transducer

For the purpose of the work, Nufern S1310 single-mode DCF was selected to host the LPG with the following characteristics: pure silica core with diameter of 8 μm, F-doped inner cladding with diameter of about 95 μm, pure silica outer cladding with diameter of 125 μm, core NA = 0.12 and MFD = 10.4 ± 0.8 μm at λ = 1550 nm. For the grating inscription, we used a well-settled platform based on the electric arc discharge (EAD) method (Esposito et al., 2018a), since this technique permits LPG fabrication in not photosensitive fibers with high flexibility. The period of the grating Λ was designed to be 400 μm in order to have the resonance corresponding to the 7th and 6th orders of cladding modes in the working wavelength range, as for the most of LPG biosensors, despite the use of an unconventional fiber (Chiavaioli et al., 2015; Esposito et al., 2018b; Quero et al., 2016). The EAD process fabrication parameters were set to arc power of 15 step (proprietary unit from Sumitomo, Japan), arc duration of 570 ms, and electrode gap of about 800 μm with the fiber stretched by a 9.8 mN force; with these parameters, it was possible to fabricate LPGs with insignificant power loss and maximum length of 30 mm to be housed in the microfluidic channel. The resulting spectrum of the grating is reported in Fig. 4 (black line) where the attenuation bands corresponding to the 5th and 6th order cladding modes can be observed at 1232 nm and 1377 nm, respectively. The bulk refractive index sensitivity was measured by surrounding the grating with liquids having calibrated refractive index with the setup reported in (Esposito et al., 2018a) and a value of −78 nm/RIU was found by considering a linear approximation in the range 1.33–1.37.

To work in mode transition region, the outer cladding diameter was decreased by using wet chemical etching in 24% (v/v) HF acid solution

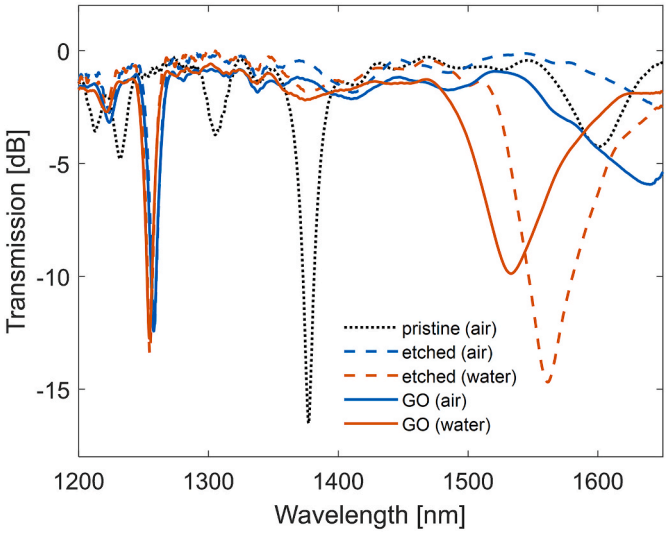

Fig. 4. Spectra of LPG in double cladding fiber (in following this grating will be named as LPG-B): after fabrication (black dotted), after etching in air (blue dashed) and water (orange dashed), after GO deposition in air (blue) and in water (orange). (For interpretation of the references to color in this figure legend, the reader is referred to the Web version of this article.)

with a 0.7 μm/min etching rate. Fig. 5(a), 5(b) and 5(c) illustrate the evolution of the LPG response as a function of the fiber diameter during the etching process, in terms of resonance wavelength, amplitude and bandwidth, respectively, of the attenuation bands related to 4th, 5th and 6th cladding modes. To support this analysis, the results of numerical simulations using the model from (Esposito et al, 2018b, 2020b) are also detailed in the same figures with solid lines, showing a satisfactory agreement with the experimental data, except for few regions. The main effects due to the decrease in the fiber diameter are the shift of the resonance of all bands towards longer wavelengths and the decrease in the resonance amplitude of almost all bands (i.e. increase in the peak depth) according to previous studies of LPG in standard fiber (Iadicicco et al., 2007). Moreover, slight changes are evident in the resonance bandwidths, except for some regions where an increasing behavior of these is observed. All figures reveal that 6th cladding mode moves towards outside of the investigated wavelength range, when the fiber diameter reaches 120 μm (with slight disagreement in comparison to numerical result), whereas the 4th cladding mode becomes visible for diameters lower than 117 μm. Moreover, it is worth pointing out that the shift rate is maximum when a modal transition phenomenon occurs. Two transition regions can be identified in Fig. 5(a); as far as the 5th cladding mode is concerned, they occur for diameter values around 116 μm and 107 μm, represented by the shadowed regions. Here the resonance wavelength of the *i*-th order cladding mode shifts versus the one of the (*i*+1)-th and so on (Cusano et al., 2006; Esposito et al., 2020b). Moreover, during the modal transition, the resonance amplitude (Fig. 5 (b)) and bandwidth (Fig. 5(c)) experienced a decrease and a widening, respectively, even if the attenuation band remained very well visible. This behavior was not observed in the numerical curves and can be attributed to irregularities in the grating structure. Moreover, soon after transition (for instance when diameter is around 113 μm) the resonance amplitude and bandwidth of 5th cladding mode (red line) changed to match those of the 6th cladding mode (green curve). An unexpected effect (but repeatable for all investigated gratings) is visible far from the transitions: a decrease and a widening of the resonance amplitude and bandwidth occur, respectively, when fiber diameter is around 118 μm and 110 μm. Even if the reason is still under investigation, it can be ascribed to defects of the grating structure due to the fabrication process. However, such regions are far from the operating point selected in this work, and hence they did not affect the final results.

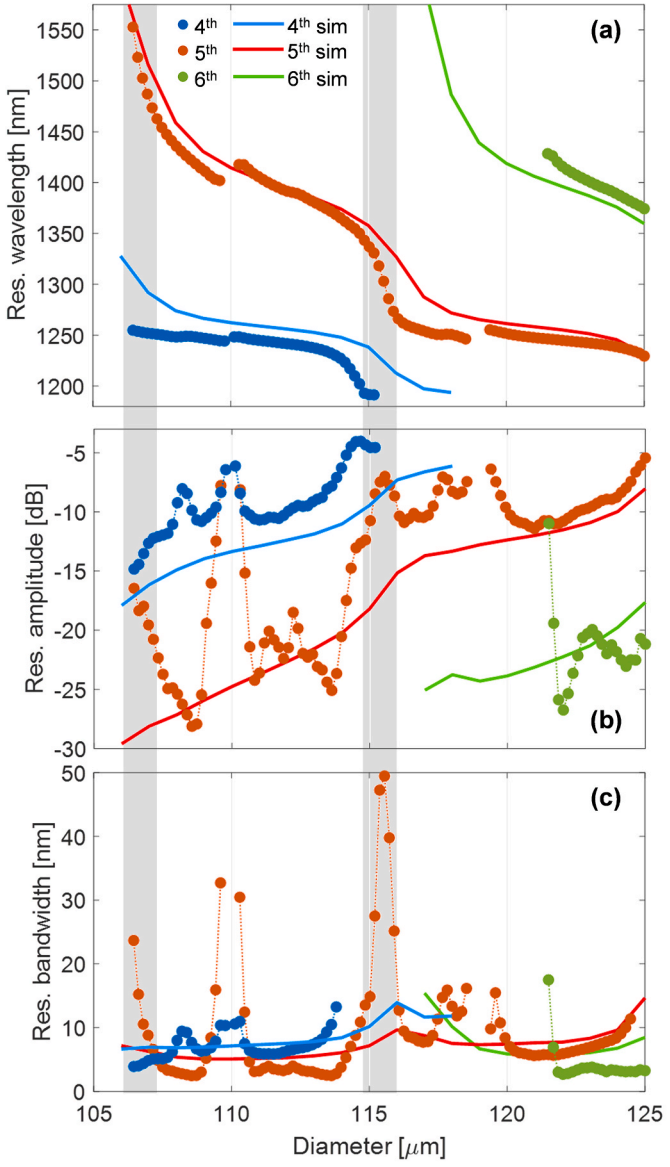

Fig. 5. Effect of changing the fiber diameter during the etching process on the resonance: (a) wavelengths; (b) amplitudes; (c) 3-dB bandwidths. Markers are related to the experimental data of 6th (green), 5th (orange) and 4th (blue) orders of cladding modes. Simulation data are reported with solid lines and same color code. (For interpretation of the references to color in this figure legend, the reader is referred to the Web version of this article.)

The etching process was thus stopped at the mode transition around 107 μm to enhance the SRI sensitivity in water-like environment. The spectra after the etching process are plotted in Fig. 4: spectrum in air (blue dashed line) exhibits an attenuation band beyond 1650 nm (i.e. the limit of our interrogation setup) whereas the resonance band in water (orange dashed line) is centered at 1561 nm with depth of 15 dB and bandwidth of 22 nm. The polarization dependence of the etched LPG in water environment was also evaluated according to (Esposito et al., 2019) and a maximum polarization dependent loss, PDL_{max}, not higher than 5 dB was found.

Subsequently, the grating was coated with a few nanometer thin layer of GO for the creation of functional groups on its surface, by using the procedure reported in section 2.2 (Esposito et al., 2018b). Fig. 4 shows the spectra of the LPG in air and water after GO deposition with blue and orange solid lines, respectively. Regarding the latter, a resonance band centered at 1533 nm with depth of 10 dB and bandwidth of 43 nm can be observed: the peak depth in water environment decreased significantly. Moreover, we believe that the GO layer slightly affects the SRI sensitivity, even if it has refractive index of 1.8–2.0, because of the low thickness.

For comparison, a second LPG was fabricated in a similar manner, but in this case the etching process was stopped for a fiber diameter slightly higher (108 μm), which resulted in a working point less close to transition region. In the following, the devices are named LPG-B and LPG-A for the former and the latter reported, respectively. The final SRI sensitivities (before GO) in water environment were found to be equal to −1035 nm/RIU (13 times sensitivity gain due to etching) and −670 nm/RIU (10 times sensitivity gain) for LPG-B and LPG-A, respectively, by considering a linear approximation in the range 1.33–1.37. After the GO deposition, no further SRI characterization was carried out to preserve the GO surface properties. In fact, it is important to observe that it is advantageous to keep the GO layer as thin as possible because its non-negligible absorption coefficient affects the visibility of the attenuation band.

Finally, a third LPG (hereinafter named LPG-C) was fabricated with the same parameters and procedures used for LPG-B. This device played the role of assessing the repeatability and reproducibility of the entire process as previously mentioned.

In the following steps, such as biosensing layer preparation and CRP detection, the devices were placed inside the microfluidic system as described in section 2.4.

3.2. Sensing bio-layer preparation

Fig. 6 details the response of the sensor (i.e. sensorgram) - resonance wavelength vs time - for the three devices, LPG-A (in orange), LPG-B (in blue) and LPG-C (in grey), during all the steps described in Section 2.5 for the preparation of the biosensing layer. The solution containing the capture antibody (anti-CRP) is allowed to flow for roughly 1 h following a standard protocol already used in the past (Chiavaioli et al., 2014a, 2015, 2018). It is worthy to observe that, except for the change of the signal due to a higher RI of BSA with respect to that of PBS, the surface passivation seems to be not so effective. In fact, the signal does not change before and after the PBS injection, which means that the available surface for the immobilization of the receptor is totally covered with a very low probability of non-specific binding interaction. This is also proved in Fig. 7 where a solution of diluted human serum is used as specificity test with a negligible change of the signal before and after the PBS injection; the residual shifts in all cases were of the order of the maximum experimental error (0.016 nm).

It should be pointed out that the sudden change in the signal before the immobilization of the capture antibody (anti-CRP) was due to the fact that the sensor was exposed to air for a few seconds in order to remove the air bubbles formed during the previous step. After that, everything took place regularly with the sensor always immersed in solution at a constant flow rate according to the values provided in Section 2.5.

3.3. Detection of CRP

The response of the three devices during the calibration phase with CRP solutions at increasing concentrations as specific target analyte is shown in Fig. 7. In the sensorgrams, the first step refers to the specificity test with a solution of free-CRP human serum used as a negative control (blank measurement). Human serum is a highly complex biological matrix constituted by more than 10,000 different kinds of proteins, and is routinely used as clinically-validating procedure (Nanjappa et al., 2014). In this case, the variation of the signal measured in PBS after rinsing was negligible and within the limits of variation of the signal (standard deviation) considering the SNR of the system, thus guaranteeing a good specificity of the biosensor (Chiavaioli et al., 2017b). After that, the residual wavelength shifts measured in PBS after rinsing reflect the amount of CRP that binds when increasing concentrations of the target analyte are injected into the microfluidic system.

It could be noted from Fig. 7 that, differently from the other experiments, the LPG-B resonance wavelength increased immediately following by a slowly decrease when CRP solutions were injected. This might be relied on the effect of temperature stabilization inside the microfluidic system that implied a longer time for the injected solutions to reach the temperature set by the control system, since the CRP solutions were stored in the refrigerator and taken out just before their use. As mentioned in section 2.5, to overcome this issue, the duration of the steps for the analyte injection and the subsequent rinsing in PBS was lengthened with respect to LPG-A. In particular, the time to reach the stable condition during the injection of the CRP solution increased of about 10 min. Moreover, during the experiments with LPG-C, to avoid any problem, CRP solutions were taken out from the refrigerator some minutes before starting the detection procedure. Another issue to observe is the fact that the LPG-A resonance wavelength experienced a slowly increase during the washing steps in PBS, while this didn't happen with the other sensors where a stable condition (i.e. steady-state) was attained. It can be ascribed to flow-induced bending on the grating due to high flow rate used during the washing steps. Furthermore, the gluing procedure of LPG-B and LPG-C into the microfluidic system was optimized by applying a slight pre-strain state along the fiber. Since the temperature was the same for all the LPGs, a comparison between the performances of the three sensors could be effectively performed. However, it is worth pointing out that the experiment with LPG-A (first experiment) can be considered as a proof-of-concept for the use of DCFs coated with GO as biosensors.

In all cases, it is evident that the sensor response moved monotonically towards shorter wavelengths with increasing CRP concentration, thus in agreement with the sensing mechanism of the optical transducer used (Chiavaioli et al., 2017a; Esposito et al., 2018b; James

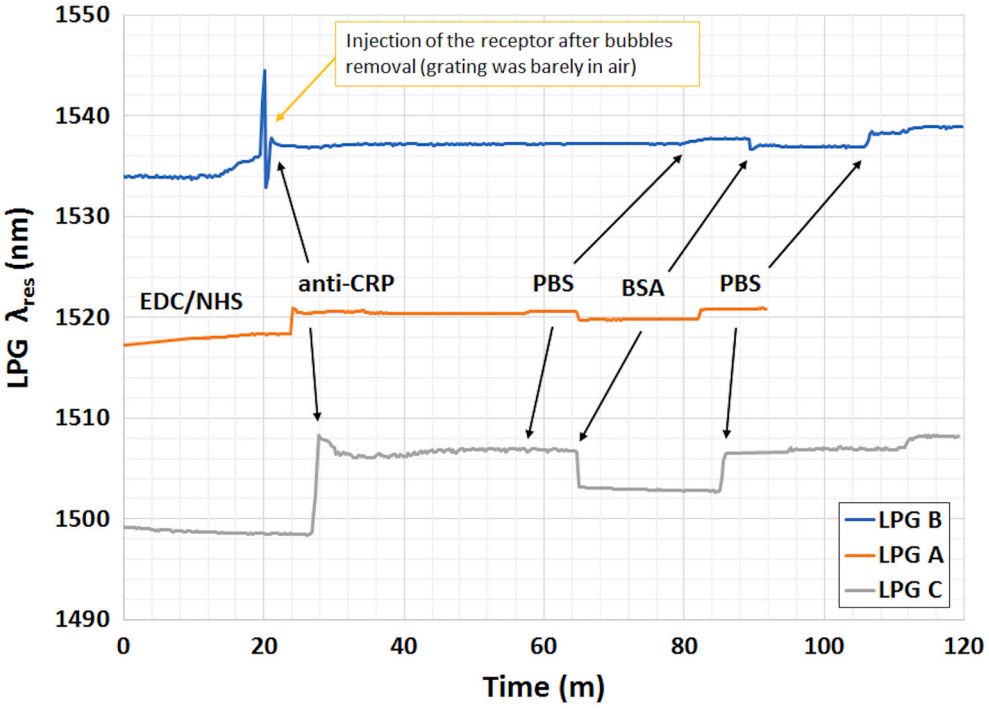

Fig. 6. Real-time response of LPG-A (orange line), LPG-B (blue line) and LPG-C (grey line), during the preparation of the biosensing layer with the immobilization of the biological recognition element (anti-CRP). (For interpretation of the references to color in this figure legend, the reader is referred to the Web version of this article.)

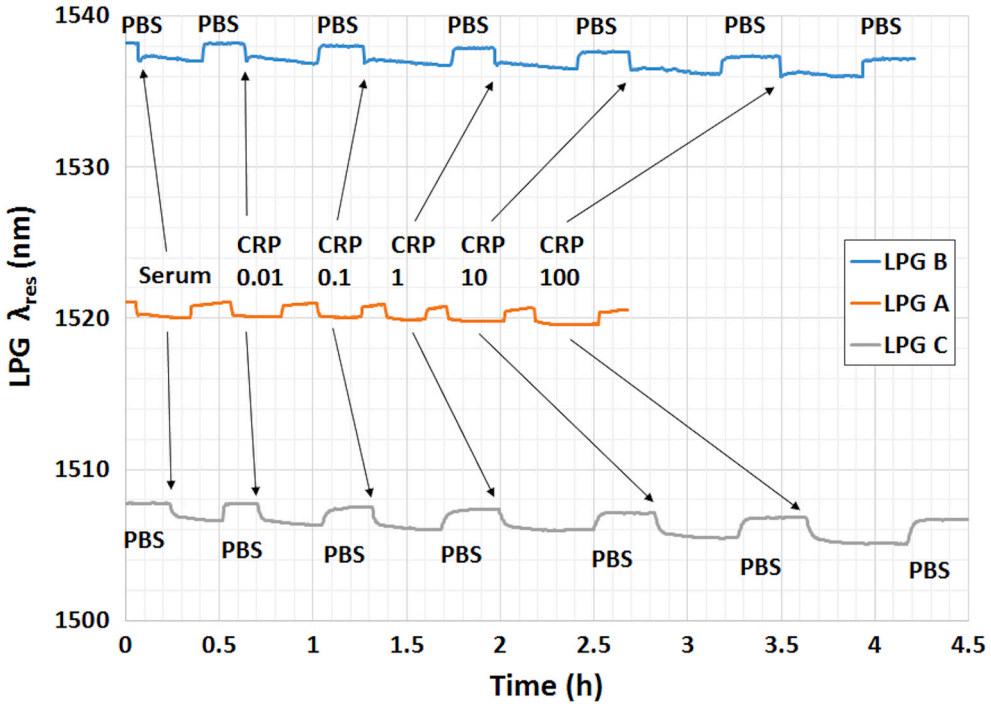

Fig. 7. Real-time response of LPG-A (orange line), LPG-B (blue line) and LPG-C (grey line), during the injection of the specific target analyte (CRP) at increasing concentrations (reported in μg/mL). The first step details the injection of a solution of human serum as negative control for the specificity test. (For interpretation of the references to color in this figure legend, the reader is referred to the Web version of this article.)

and Tatam, 2003; Shu et al., 2002).

The calibration curves for the three devices drawn in semi-log scale are shown in Fig. 8(a). The resonance wavelengths (for all LPGs) have been scaled down with respect to the initial value of the baseline (i.e. the residual shift), and the mean value and the associated standard deviation for 20 subsequent measurements (black error bars) are displayed for each experimental point (for better clarity and direct comparison, in Fig. 8(a) for LPG-A and in Fig. 8(b) for the other two LPGs). It should be pointed out that the experimental points showed in the calibration curves (Fig. 8) refer to a single independent experiment without any regeneration. The fitting of the experimental data by using the Logistic function is also reported as dashed curves. It was extrapolated from the Langmuir isotherm model, which is a well-accepted mathematical model capable to take into account the degree of interaction between ligand binding sites (Dudley et al., 1985), as also detailed in the literature (Chiavaioli et al., 2014b). Here, the Logistic function is profitably expressed in terms of wavelength shift $\Delta\lambda$ as:

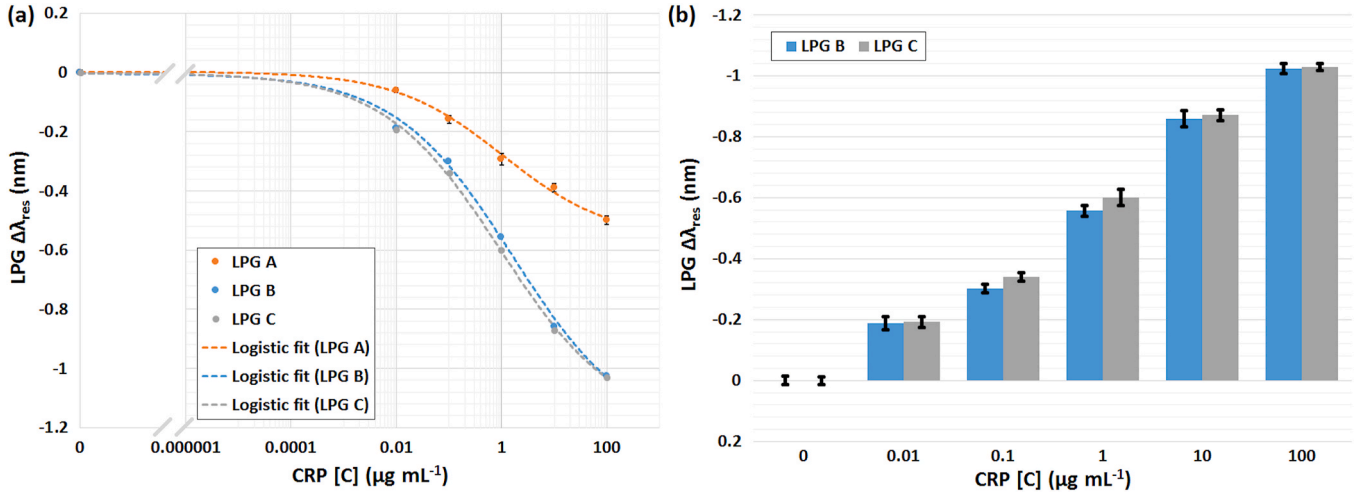

Fig. 8. (a) Semi-log calibration curves of LPG-A (orange), LPG-B (blue) and LPG-C (grey), obtained from the respective sensorgrams of Fig. 7. Each concentration of CRP (circles) is expressed in terms of the mean value and the respective standard deviation within 20 measurements showed for LPG-A (black error bars). The dashed curves (orange for LPG-A, blue for LPG-B and grey for LPG-C) represent the fitting of the experimental data by using the Logistic function. (b) Comparative histogram of the results attained for the detection of CRP with two independent and repeated experiments using LPG-B (blue) and LPG-C (grey). Each column represents the mean value of the signal, together with the respective standard deviation within 20 measurements (black error bars). (For interpretation of the references to color in this figure legend, the reader is referred to the Web version of this article.)

$$\Delta\lambda = -\Delta\lambda_{MAX} \cdot \left[\frac{\left(\frac{x}{x_0}\right)^p}{1+\left(\frac{x}{x_0}\right)^p} \right] \quad (2)$$

where $\Delta\lambda_{MAX}$ accounts for the difference between the asymptotes of the sigmoidal curve, and hence represents the dynamic signal change (also named dynamic range), x_0 is the value of the analyte concentration for which the value of LPG resonance wavelength shift is equal to 50% of the dynamic range and p is a coefficient that is related to the slope of the sigmoidal curve for $x = x_0$. As a matter of fact, it is expected that the first parameter of Eq. (2) changes proportionally to the sensitivity of the sensor, whilst x_0 and p should be comparable for all LPGs, since they depend on the binding interaction between anti-CRP and CRP (i.e. on the assay protocol). For a direct comparison and in order to assess the biosensor repeatability and reproducibility, Fig. 8(b) accounts for the histogram of the results extrapolated from Fig. 8(a) for the detection of CRP with two independent experiments using LPG-B (blue) and LPG-C (grey). Each column represents the mean value of the signal, together with the respective standard deviation within subsequent 20 measurements (black error bars). Table 1 gathers all the fitting parameters for the three devices. The high correlation coefficient R^2 proves the effectiveness of the fitting procedure. As expected, x_0 and p are quite similar (within the error) for all LPGs, thus testifying the same interaction mechanism, whereas $\Delta\lambda_{MAX}$ is significantly higher for LPG-B and LPG-C than that for LPG-A due to the improved sensitivity. Those results can be considered very remarkable in biosensing, taking into account all the involved variables, and underpin the effectiveness of the proposed biosensing platform.

According to the literature (Chiavaioli et al., 2017b), a series of parameters of interest can be derived from the calibration curve to assess the performance of the biosensor. Among them, the LOD, defined as the variation of the signal relating to the concentration 0 of the analyte (blank measurement) plus three times its standard deviation, is certainly one of the most important. In this case, a LOD of about 1.1 ng/mL ($3\sigma \cong 0.026$ nm) is attained with LPG-A. Despite a slightly larger standard deviation ($3\sigma \cong 0.042$ nm for LPG-B and $3\sigma \cong 0.037$ nm for LPG-C) as expected from the spectral features of the resonance, a LOD of about 0.32 ng/mL and 0.15 ng/mL is attained with LPG-B and LPG-C, respectively, a value roughly 60-fold lower (LPG-C) than that reported in the literature using the same assay protocol based on the anti-CRP/CRP interaction, but making use of an optical transducer based on the SPR phenomenon (Aray et al., 2016). While the LOD attained is not the lowest reported in the literature (Schulze et al., 2018), it should be pointed out that the results here described have been achieved with a complex matrix of human serum and in repeated independent experiments, and the robustness and practical usage of the optical transducer could be a critical issue to consider in the case of extremely etched or very complicated in-fiber devices. Moreover, from Fig. 8, a total wavelength shift of 0.49 nm, 1.02 nm and 1.03 nm for CRP concentrations varying from 0 to 100 μg/mL is obtained with LPG-A, LPG-B and LPG-C, respectively. In addition, the surface sensitivity can be calculated (Chiavaioli et al., 2017b) if the CRP concentration is reported in linear scale like the classical Langmuir isotherm model, by applying a linear regression approach from the blank measurement up to 0.01 μg/mL CRP where the linearity is maintained. This calculation leads to the values of −19.22 nm/(μg/mL), −18.63 nm/(μg/mL) and −8.58 nm/(μg/mL) for LPG-C, LPG-B and LPG-A, respectively. Finally, another interesting parameter was evaluated, which is the working range of the biosensor defined as the CRP concentration range between 10% and 90% of the dynamic range ($\Delta\lambda_{MAX}$) (Chiavaioli et al., 2014b). The proposed biosensing device can cover a large working range (1 ng/mL – 100 μg/mL) of clinical relevance.

Table 1
Parameters of fitting curves related to the experimental data of LPG-A, LPG-B and LPG-C.

Sensor name	R^2	$\Delta\lambda_{MAX}$ (nm)	x_0 (μg/mL)	p
LPG-A	0.9938	0.5664 ± 0.0620	1.07 ± 0.6644	0.4238 ± 0.0606
LPG-B	0.9957	1.1319 ± 0.1302	1.6125 ± 0.9603	0.3899 ± 0.0573
LPG-C	0.9987	1.1969 ± 0.1542	1.2488 ± 0.3217	0.3931 ± 0.0348

Given the reported values of LOD and working range, it is important to point out that a common laboratory practice is to dilute the body-fluid sample (i.e. serum, plasma, etc.) in order to minimize the matrix-effect of not specific adsorption onto the surface of the sensing area. The applied dilution is generally 1:10, but can be even down to 1:100, leading, consequently, to a decrease of one (1:10) or two (1:100) orders of magnitude of the clinical range. Taking into account that the level of CRP in serum in healthy Caucasian people is estimated to be around 0.8 μg/mL, a LOD of 0.08 μg/mL or 0.008 μg/mL should be considered in case of dilution of 1:10 and 1:100, respectively. With this in mind, the low LOD and the wide working range attained with the proposed devices are perfectly justified.

4. Conclusions

In this work, we have proposed a novel fiber-optic based biosensor which was tested for the real-time label free detection of C-reactive protein in serum. It is based on an unconventional LPG fabricated in W-type double cladding fiber by EAD technique. Here, the working point of the device was tuned to mode transition region by slight etching of the fiber outer cladding, in order to attain significant enhancement of the sensitivity and at the same time preserving the visibility of the grating spectral features (and thus SNR). In addition, due to absence of additional buffer layers, the so-prepared LPGs, consisting of all-silica structure tuned in modal transition, guarantee stability and long-term use with similar spectral and sensitivity features. Moreover, fiber transducer was coated with a nanometric thin layer of GO exhibiting oxygen-containing functional groups, which were used for the covalent immobilization of the capture antibody. The device was tested using a state-of-the-art microfluidic system for fiber-optic biosensors and the achieved results were analyzed by considering a series of parameters of interest. The device was applied for the detection of CRP concentrations in serum of clinical relevance. In the best case, a LOD of about 0.15 ng/mL was obtained, which is one of the lowest reported so far in literature concerning fiber-optic biosensors, and the device is able to cover a large working range (1 ng/mL – 100 μg/mL) of clinical relevance. Finally, the repeatability and reproducibility of the entire process, encompassing device fabrication, assay protocol and device response, were taken into account by carrying out independent tests in the same experimental conditions. The achieved results can be considered very remarkable in biosensing, taking into account all the involved variables, and underpin the effectiveness of the proposed biosensing platform.

CRediT authorship contribution statement

Flavio Esposito: Conceptualization, Investigation, Resources, Writing - original draft. **Lucia Sansone:** Investigation, Resources, Writing - original draft. **Anubhav Srivastava:** Investigation, Resources. **Francesco Baldini:** Supervision, Writing - review & editing. **Stefania Campopiano:** Conceptualization, Supervision, Writing - review & editing. **Francesco Chiavaioli:** Conceptualization, Validation, Formal analysis, Investigation, Writing - original draft. **Michele Giordano:** Conceptualization, Investigation, Formal analysis, Writing - review & editing. **Ambra Giannetti:** Conceptualization, Resources, Writing - original draft. **Agostino Iadicicco:** Conceptualization, Investigation, Formal analysis, Writing - review & editing.

Declaration of competing interest

The authors declare that they have no known competing financial interests or personal relationships that could have appeared to influence the work reported in this paper.

References

Aray, A., Chiavaioli, F., Arjmand, M., Trono, C., Tombelli, S., Giannetti, A., Cennamo, N., Soltanolkotabi, M., Zeni, L., Baldini, F., 2016. SPR-based plastic optical fibre biosensor for the detection of C-reactive protein in serum. J. Biophot. 9, 1077–1084. https://doi.org/10.1002/jbio.201500315.

Berneschi, S., Baldini, F., Cosci, A., Farnesi, D., Nunzi Conti, G., Tombelli, S., Trono, C., Pelli, S., Giannetti, A., 2017. Fluorescence biosensing in selectively photo–activated microbubble resonators. Sensor. Actuator. B Chem. 242, 1057–1064. https://doi.org/10.1016/j.snb.2016.09.146.

Biswas, P., Dey, T.K., Basumallick, N., Bandyopadhyay, Sankhyabrata, Ghosh, A., Bandyopadhyay, Somnath, 2016. Realization of high sensitive refractive index sensor with enhanced contrast using an over coupled long period fiber grating operating at mode transition. In: 13th International Conference on Fiber Optics and Photonics. OSA, Washington, D.C.. https://doi.org/10.1364/PHOTONICS.2016.Tu3G.4. Tu3G.4.

Chiavaioli, F., Biswas, P., Trono, C., Bandyopadhyay, S., Giannetti, A., Tombelli, S., Basumallick, N., Dasgupta, K., Baldini, F., 2014a. Towards sensitive label-free immunosensing by means of turn-around point long period fiber gratings. Biosens. Bioelectron. 60, 305–310. https://doi.org/10.1016/j.bios.2014.04.042.

Chiavaioli, F., Baldini, F., Tombelli, S., Trono, C., Giannetti, A., 2017a. Biosensing with optical fiber gratings. Nanophotonics 6, 663–679. https://doi.org/10.1515/nanoph-2016-0178.

Chiavaioli, F., Biswas, P., Trono, C., Jana, S., Bandyopadhyay, S., Basumallick, N., Giannetti, A., Tombelli, S., Bera, S., Mallick, A., Baldini, F., 2015. Sol–gel-based titania–silica thin film overlay for long period fiber grating-based biosensors. Anal. Chem. 87, 12024–12031. https://doi.org/10.1021/acs.analchem.5b01841.

Chiavaioli, F., Gouveia, C., Jorge, P., Baldini, F., 2017b. Towards a uniform metrological assessment of grating-based optical fiber sensors: from refractometers to biosensors. Biosensors 7, 23. https://doi.org/10.3390/bios7020023.

Chiavaioli, F., Zubiate, P., Del Villar, I., Zamarreño, C.R., Giannetti, A., Tombelli, S., Trono, C., Arregui, F.J., Matias, I.R., Baldini, F., 2018. Femtomolar detection by nanocoated fiber label-free biosensors. ACS Sens. 3, 936–943. https://doi.org/10.1021/acssensors.7b00918.

Chiavaioli, F., Trono, C., Giannetti, A., Brenci, M., Baldini, F., 2014b. Characterisation of a label-free biosensor based on long period grating. J. Biophot. 7, 312–322. https://doi.org/10.1002/jbio.201200135.

Clarke, J.L., Anderson, J.L., Carlquist, J.F., Roberts, R.F., Horne, B.D., Bair, T.L., Kolek, M.J., Mower, C.P., Crane, A.M., Roberts, W.L., Muhlestein, J.B., 2005. Comparison of differing C-reactive protein assay methods and their impact on cardiovascular risk assessment. Am. J. Cardiol. 95, 155–158. https://doi.org/10.1016/j.amjcard.2004.08.087.

Cusano, A., Iadicicco, A., Pilla, P., Contessa, L., Campopiano, S., Cutolo, A., Giordano, M., 2006. Mode transition in high refractive index coated long period gratings. Optic Express 14, 19–34. https://doi.org/10.1364/OPEX.14.000019.

Del Villar, I., 2015. Ultrahigh-sensitivity sensors based on thin-film coated long period gratings with reduced diameter, in transition mode and near the dispersion turning point. Optic Express 23, 8389–8398. https://doi.org/10.1364/OE.23.008389.

Del Villar, I., Matias, I.R., Arregui, F.J., Achaerandio, M., 2005. Nanodeposition of materials with complex refractive index in long-period fiber gratings. J. Lightwave Technol. 23, 4192–4199. https://doi.org/10.1109/JLT.2005.858246.

Dominici, R., Luraschi, P., Franzini, C., 2004. Measurement of C-reactive protein: two high sensitivity methods compared. J. Clin. Lab. Anal. 18, 280–284. https://doi.org/10.1002/jcla.20038.

Dudley, R.A., Edwards, P., Ekins, R.P., Finney, D.J., McKenzie, I.G., Raab, G.M., Rodbard, D., Rodgers, R.P., 1985. Guidelines for immunoassay data processing. Clin. Chem. 31, 1264–1271. https://doi.org/10.1093/clinchem/31.8.1264.

Esposito, F., Campopiano, S., Iadicicco, A., 2019. Arc-induced long period gratings in erbium-doped fiber. IEEE Photonics J 11, 1–8. https://doi.org/10.1109/JPHOT.2019.2894300.

Esposito, F., Ranjan, R., Campopiano, S., Iadicicco, A., 2018a. Arc-induced long period gratings from standard to polarization-maintaining and photonic crystal fibers. Sensors 18, 918. https://doi.org/10.3390/s18030918.

Esposito, F., Sansone, L., Taddei, C., Campopiano, S., Giordano, M., Iadicicco, A., 2018b. Ultrasensitive biosensor based on long period grating coated with polycarbonate-graphene oxide multilayer. Sensor. Actuator. B Chem. 274, 517–526. https://doi.org/10.1016/j.snb.2018.08.002.

Esposito, F., Srivastava, A., Sansone, L., Giordano, M., Campopiano, S., Iadicicco, A., 2020a. Label-free biosensors based on long period fiber gratings: a review. IEEE Sensor. J. https://doi.org/10.1109/JSEN.2020.3025488.

Esposito, F., Srivastava, A., Sansone, L., Giordano, M., Campopiano, S., Iadicicco, A., 2020b. Sensitivity enhancement in long period gratings by mode transition in uncoated double cladding fibers. IEEE Sensor. J. 20, 234–241. https://doi.org/10.1109/JSEN.2019.2942639.

Giannetti, A., Trono, C., Porro, G., Domenici, C., Puntoni, M., Baldini, F., 2020. Towards an integrated system as point-of-care device for the optical detection of sepsis biomarkers. Chemosensors 8, 12. https://doi.org/10.3390/chemosensors8010012.

Giordano, M., Baldini, F., Campopiano, S., Chiavaioli, F., Esposito, F., Giannetti, A., Iadicicco, A., Sansone, L., Srivastava, A., 2020. Trasduttore in fibra ottica chimicamente funzionalizzato per la sensoristica. IT Patent pending nr, 102020000005062.

Hage, F.G., Szalai, A.J., 2007. C-reactive protein gene polymorphisms, C-reactive protein blood levels, and cardiovascular disease risk. J. Am. Coll. Cardiol. 50, 1115–1122. https://doi.org/10.1016/j.jacc.2007.06.012.

Hernaez, M., Zamarreño, C., Melendi-Espina, S., Bird, L., Mayes, A., Arregui, F., 2017. Optical fibre sensors using graphene-based materials: a review. Sensors 17, 155. https://doi.org/10.3390/s17010155.

Hummers, W.S., Offeman, R.E., 1958. Preparation of graphitic oxide. J. Am. Chem. Soc. 80, 1339. https://doi.org/10.1021/ja01539a017.

Iadicicco, A., Campopiano, S., Giordano, M., Cusano, A., 2007. Spectral behavior in thinned long period gratings: effects of fiber diameter on refractive index sensitivity. Appl. Optic. 46, 6945–6952. https://doi.org/10.1364/AO.46.006945.

Islam, M.S., Kang, S.H., 2011. Chemiluminescence detection of label-free C-reactive protein based on catalytic activity of gold nanoparticles. Talanta 84, 752–758. https://doi.org/10.1016/J.TALANTA.2011.02.001.

James, S.W., Tatam, R.P., 2003. Optical fibre long-period grating sensors: characteristics and application. Meas. Sci. Technol. 14, R49–R61. https://doi.org/10.1088/0957-0233/14/5/201.

Lichtenberg, J.Y., Ling, Y., Kim, S., 2019. Non-specific adsorption reduction methods in biosensing. Sensors 19, 2488. https://doi.org/10.3390/s19112488.

Liu, C., Xu, B.J., Zhou, L., Sun, Z., Mao, H.J., Zhao, J.L., Zhang, L., Chen, X., 2018. Graphene oxide functionalized long period fiber grating for highly sensitive hemoglobin detection. Sensor. Actuator. B Chem. 261, 91–96. https://doi.org/10.1016/j.snb.2018.01.117.

Liu, Y., Dong, X., Chen, P., 2012. Biological and chemical sensors based on graphene materials. Chem. Soc. Rev. 41, 2283. https://doi.org/10.1039/c1cs15270j.

Loh, K.P., Bao, Q., Eda, G., Chhowalla, M., 2010. Graphene oxide as a chemically tunable platform for optical applications. Nat. Chem. 2, 1015–1024. https://doi.org/10.1038/nchem.907.

Luan, Y., Yao, Y., 2018. The clinical significance and potential role of C-reactive protein in chronic inflammatory and neurodegenerative diseases. Front. Immunol. 9 https://doi.org/10.3389/fimmu.2018.01302.

Nanjappa, V., Kurian Thomas, J., Marimuthu, A., Muthusamy, B., Radhakrishnan, A., Sharma, R., Ahmad Khan, A., Balakrishnan, L., Sahasrabuddhe, N.A., Kumar, S., Nitinbhai Jhaveri, B., Vinaykumar Sheth, K., Kumar Khatana, R., Shaw, P.G., Manda Srikanth, S., Mathur, P.P., Shankar, S., Nagaraja, D., Christopher, R., Mathivanan, S., Raju, R., Sirdeshmukh, R., Chatterjee, A., Simpson, R.J., Harsha, H.C., Pandey, A., Keshava Prasad, T.S., 2014. Plasma Proteome Database as a resource for proteomics research: 2014 update. Nucleic Acids Res. 42, D959–D965. https://doi.org/10.1093/nar/gkt1251.

Nathan, C., Ding, A., 2010. Nonresolving inflammation. Cell 140, 871–882. https://doi.org/10.1016/j.cell.2010.02.029.

Parra, M.D., Tuomola, M., Cabezas-Herrera, J., Ceron, J.J., 2005. Use of a time-resolved immunofluorometric assay for determination of canine C-reactive protein concentrations in whole blood. Am. J. Vet. Res. 66, 62–66. https://doi.org/10.2460/ajvr.2005.66.62.

Pisco, M., Cusano, A., 2020. Lab-on-fiber technology: a roadmap toward multifunctional plug and play platforms. Sensors 20, 4705. https://doi.org/10.3390/s20174705.

Quero, G., Consales, M., Severino, R., Vaiano, P., Boniello, A., Sandomenico, A., Ruvo, M., Borriello, A., Diodato, L., Zuppolini, S., Giordano, M., Nettore, I.C., Mazzarella, C., Colao, A., Macchia, P.E., Santorelli, F., Cutolo, A., Cusano, A., 2016. Long period fiber grating nano-optrode for cancer biomarker detection. Biosens. Bioelectron. 80, 590–600. https://doi.org/10.1016/j.bios.2016.02.021.

Rourke, J.P., Pandey, P.A., Moore, J.J., Bates, M., Kinloch, I.A., Young, R.J., Wilson, N. R., 2011. The real graphene oxide revealed: stripping the oxidative debris from the graphene-like sheets. Angew. Chem. Int. Ed. 50, 3173–3177. https://doi.org/10.1002/anie.201007520.

Salvo, P., Dini, V., Kirchhain, A., Janowska, A., Oranges, T., Chiricozzi, A., Lomonaco, T., Di Francesco, F., Romanelli, M., 2017. Sensors and biosensors for C-reactive protein, temperature and pH, and their applications for monitoring wound healing: a review. Sensors 17, 2952. https://doi.org/10.3390/s17122952.

Schulze, S., Wehrhold, M., Hille, C., 2018. Femtosecond-pulsed laser written and etched fiber Bragg gratings for fiber-optical biosensing. Sensors 18, 2844. https://doi.org/10.3390/s18092844.

Shu, X., Zhang, L., Bennion, I., 2002. Sensitivity characteristics of long-period fiber gratings. J. Lightwave Technol. 20, 255–266. https://doi.org/10.1109/50.983240.

Śmietana, M., Koba, M., Mikulic, P., Bock, W.J., 2016. Towards refractive index sensitivity of long-period gratings at level of tens of μm per refractive index unit: fiber cladding etching and nano-coating deposition. Optic Express 24, 11897–11904. https://doi.org/10.1364/OE.24.011897.

Sproston, N.R., Ashworth, J.J., 2018. Role of C-reactive protein at sites of inflammation and infection. Front. Immunol. 9, 754. https://doi.org/10.3389/fimmu.2018.00754.

Sridevi, S., Vasu, K.S., Asokan, S., Sood, A.K., 2015. Sensitive detection of C-reactive protein using optical fiber Bragg gratings. Biosens. Bioelectron. 65, 251–256. https://doi.org/10.1016/j.bios.2014.10.033.

Vaiano, P., Carotenuto, B., Pisco, M., Ricciardi, A., Quero, G., Consales, M., Crescitelli, A., Esposito, E., Cusano, A., 2016. Lab on Fiber Technology for biological sensing applications. Laser Photon. Rev. 10, 922–961. https://doi.org/10.1002/lpor.201600111.

Wang, L., 2020. C-reactive protein levels in the early stage of COVID-19. Med. Maladies Infect. 50, 332–334. https://doi.org/10.1016/j.medmal.2020.03.007.

Wang, W., Mai, Z., Chen, Y., Wang, J., Li, L., Su, Q., Li, X., Hong, X., 2017. A label-free fiber optic SPR biosensor for specific detection of C-reactive protein. Sci. Rep. 7, 16904. https://doi.org/10.1038/s41598-017-17276-3.

Wang, Y., Li, Z., Wang, J., Li, J., Lin, Y., 2011. Graphene and graphene oxide: biofunctionalization and applications in biotechnology. Trends Biotechnol. https://doi.org/10.1016/j.tibtech.2011.01.008.

Xu, B., Huang, J., Ding, L., Cai, J., 2020. Graphene oxide-functionalized long period fiber grating for ultrafast label-free glucose biosensor. Mater. Sci. Eng. C 107, 110329. https://doi.org/10.1016/j.msec.2019.110329.

Zhu, Y., Murali, S., Cai, W., Li, X., Suk, J.W., Potts, J.R., Ruoff, R.S., 2010. Graphene and graphene oxide: synthesis, properties, and applications. Adv. Mater. 22, 3906–3924. https://doi.org/10.1002/adma.201001068.

Zubiate, P., Urrutia, A., Zamarreño, C.R., Egea-Urra, J., Fernández-Irigoyen, J., Giannetti, A., Baldini, F., Díaz, S., Matias, I.R., Arregui, F.J., Santamaría, E., Chiavaioli, F., Del Villar, I., 2019. Fiber-based early diagnosis of venous thromboembolic disease by label-free D-dimer detection. Biosens. Bioelectron. X 2, 100026. https://doi.org/10.1016/j.biosx.2019.100026.

Zubiate, P., Zamarreño, C.R., Sánchez, P., Matias, I.R., Arregui, F.J., 2017. High sensitive and selective C-reactive protein detection by means of lossy mode resonance based optical fiber devices. Biosens. Bioelectron. 93, 176–181. https://doi.org/10.1016/j.bios.2016.09.020.

Thermofisher Scientific, Thermofisher Scientific, n.d. CRP human ELISA kit [WWW Document]. URL, www.thermofisher.com/elisa/product/CRP-Human-ELISA-Kit/KHA0031.